Stanford Exploration Project, Report 94, November 11, 1997, pages 61–72

Azimuth moveout + common-azimuth migration: Cost-effective prestack depth imaging of marine data

Biondo Biondi[1]

keywords: *AMO, common-azimuth, prestack depth migration*

ABSTRACT

Common-azimuth imaging can significantly reduce the cost of full-volume 3-D prestack depth imaging of marine data sets. The common-azimuth imaging procedure comprises of two steps: first, transformation of the prestack data to common azimuth data by azimuth moveout (AMO); second, imaging the transformed data by common-azimuth migration. Both these steps are computationally efficient. AMO is a partial-migration operator and thus it has narrow spatial aperture. Common-azimuth migration is based on downward-continuation of the wavefield; therefore, its computational cost increases only as the square of the image depth. In contrast, the cost of conventional Kirchhoff migration is proportional to the cube of the image depth.

Because it is a wavefield-continuation method, common-azimuth migration does not require the computation of asymptotic Green functions. Therefore, common-azimuth imaging is likely to overcome some of the accuracy problems encountered by Kirchhoff migration in the presence of complex wave-propagation phenomena. The proposed common-azimuth imaging procedure successfully depth imaged a marine data set recorded in the North Sea. These positive results suggest the application of common-azimuth imaging to velocity estimation based on wavefield focusing.

INTRODUCTION

Computational cost is a main obstacle to the the widespread use 3-D prestack depth migration for full-volume imaging. Currently, 3-D prestack migration is almost exclusively performed by Kirchhoff methods because they effectively handle the irregular and sparse geometries of 3-D prestack data. However, the computational cost of full-volume imaging by Kirchhoff migration increases by a factor proportional to the cube

[1]**email:** biondo@sep.stanford.edu

of the depth extent of the image, making the imaging of deeper targets extremely expensive. In contrast, the cost of migration methods based on the downward continuation of the wavefield increases only with the square of depth. But 3-D prestack data cannot be efficiently downward-continued by standard methods because of their irregular and sparse sampling.

Here I present a procedure for full-volume prestack imaging of marine data sets that takes advantage of the limited azimuthal range of 3-D marine data to reduce significantly the computational cost. The procedure comprises two steps. The first step transforms the recorded data into effective common-azimuth data, where the common-azimuth is the direction of the acquisition sail line. The second step images the synthesized common-azimuth data set by prestack migration based on the downward continuation of the wavefield.

To transform marine data into effective common-azimuth data, I "rotate" the prestack data using a partial-prestack migration operator called *azimuth moveout* (AMO) (Biondi et al., 1996a). The AMO operator is defined in the time-space domain, and it can be applied as an integral operator to 3-D marine data with geometry irregularities caused by cable feather and multi-streamer recording. The spatial aperture, and consequently the computational cost, of the AMO operator is approximately proportional to the azimuth rotation between the input offset vector and the output offset vector, and it is small when the azimuth rotation is small. Since the azimuths of most of the traces recorded during a marine acquisition are close to the nominal common azimuth, the cost of the AMO transformation is low.

Common-azimuth migration is based on a downward-continuation operator derived from the full 3-D prestack operator (Biondi and Palacharla, 1996). The method takes advantage of the narrow range of the source-receiver azimuth typical of marine data to propagate only a selected portion of the whole prestack wavefield. From an imaging perspective, the propagated portion of the wavefield is the main component of the wavefield.

In addition to being computationally efficient for full-volume imaging, common-azimuth migration has the advantage to be based on a recursive solution of the wave-equation, rather than on relying on the computation of asymptotic Green functions. Kirchhoff migration methods have been shown to have difficulties in accurately imaging reflectors below complex structures (Geoltrain and Brac, 1993; Godfrey et al., 1993; **?**; Albertin et al., 1996). Multi-pathing of wave propagating through complex velocity models is the main culprit for this loss of accuracy. The negative effects of multi-pathing can be ameliorated by performing the Kirchhoff summation over the most energetic arrivals, or even better, over multiple arrivals (Nichols, 1996). However, these improvements are seldom bullet-proof, while they add significantly to the computational cost and the implementation complexity of Kirchhoff migration.

The speed and robustness advantages of common-azimuth imaging compared with conventional Kirchhoff imaging are important in the context of velocity estimation, because velocity estimation often requires several imaging iterations. Furthermore, the availability of an efficient method for downward-continuing 3-D prestack data opens the possibility for the application to 3-D problems of velocity estimation methods based on the focusing of wavefield at depth (Yilmaz and Chambers, 1984; MacKay and Abma, 1992).

AZIMUTH-MOVEOUT TRANSFORMATION

Azimuth moveout is a crucial component of the proposed common-azimuth imaging procedure; it is the process necessary to transform narrow-azimuth data collected with multiple streamers into effective common-azimuth data. Although the AMO transformation to common azimuth is approximate, AMO removes much of the dip limitations that are intrinsic in standard methods to transform prestack data.

Azimuth moveout transforms 3-D prestack data with a given offset and azimuth to equivalent data with different offset and azimuth. The AMO operator is derived by collapsing in one single step the cascade of an imaging operator and a forward modeling operator (Biondi et al., 1996a). In principle, any 3-D prestack imaging operator can be used for defining AMO. AMO has been derived both as a cascade of DMO and "inverse" DMO and as the cascade of full 3-D prestack constant velocity migration and its inverse. AMO is applied after NMO, and thus velocity heterogeneities are taken into account, at least at first order, by the NMO step.

AMO is not a single-trace to single-trace transformation, but it is a partial-migration operator that moves events across midpoints according to their dip. Its impulse response is a saddle in the output midpoint domain. The shape of the saddle depends on the offset vector of the input data $\mathbf{h}_1 = h_1 \cos\theta_1 \vec{\mathbf{x}} + h_1 \sin\theta_1 \vec{\mathbf{y}} = h_1(\cos\theta_1, \sin\theta_1)$ and on the offset vector of the desired output data $\mathbf{h}_2 = h_2(\cos\theta_2, \sin\theta_2)$, where the unit vectors $\vec{\mathbf{x}}$ and $\vec{\mathbf{y}}$ point respectively in the in-line direction and the cross-line direction. The time shift to be applied to the data is a function of the difference vector $\boldsymbol{\Delta}\mathbf{m} = \Delta m(\cos\Delta\varphi, \sin\Delta\varphi)$ between the midpoint of the input trace and the midpoint of the output trace. The analytical expression of the AMO saddle is,

$$t_2\left(\boldsymbol{\Delta}\mathbf{m}, \mathbf{h}_1, \mathbf{h}_2, t_1\right) = t_1 \frac{h_2}{h_1} \sqrt{\frac{h_1^2 \sin^2(\theta_1 - \theta_2) - \Delta m^2 \sin^2(\theta_2 - \Delta\varphi)}{h_2^2 \sin^2(\theta_1 - \theta_2) - \Delta m^2 \sin^2(\theta_1 - \Delta\varphi)}}. \tag{1}$$

The traveltimes t_1 and t_2 are respectively the traveltime of the input data after NMO has been applied, and the traveltime of the results before inverse NMO has been applied.

The surface represented by equation (1) is a skewed saddle; its shape and spatial extent are controlled by the values of the absolute offsets h_1 and h_2, and by the azimuth rotation $\Delta\theta = \theta_1 - \theta_2$. Consistent with intuition, the spatial extent of the operator is maximum when $\Delta\theta = 90^\circ$ and it vanishes when offsets and azimuth rotation tend to zero. Furthermore, it can be easily verified that $t_2 = t_1$ for the zero-dip components of the data; that is, the kinematics of zero-dip data after NMO do not depend on azimuth and offset.

The expression for the AMO saddle is velocity independent, but the lateral aperture of the operator is velocity dependent. An upper bound on the spatial extent of the AMO operator is defined by the region where the expression in equation (1) is valid. This region is delimited by the parallelogram with main diagonal $(\mathbf{h}_1 + \mathbf{h}_2)$ and minor diagonal $(\mathbf{h}_1 - \mathbf{h}_2)$, as shown in Figure 1. The effective AMO aperture is often much narrower than the parallelogram and is, for given $\mathbf{h}_1$ and $\mathbf{h}_2$, a function of the minimum velocity V_{min} and the input traveltime. Because of its limited aperture, AMO is relatively inexpensive to apply.

Figure 2 shows the surface of the AMO impulse response when $t_1 = 1$ s, $h_1 = 2$ km, $h_2 = 1.8$ km, $\theta_1 = 0°$, and $\theta_2 = 30°$, and no limitations are imposed on the operator aperture. In contrast, Figure 3 shows the surface of the AMO impulse response with the same parameters as in Figure 2, but with the aperture limited by assuming a minimum velocity $V_{min} = 2$ km/s.

COMMON-AZIMUTH MIGRATION

Common-azimuth migration is the second component of the common-azimuth imaging procedure. Common-azimuth migration (Biondi and Palacharla, 1996) is based on a downward-continuation operator derived from the full 3-D prestack downward-continuation operator. Common-azimuth data sets are recursively evaluated at increasing depth levels, starting from the common-azimuth data set recorded at the surface. Common-azimuth data has zero cross-line offset, and thus it is only four-dimensional. Consequently, the common-azimuth operator is also only four dimensional, whereas the full 3-D prestack downward continuation operator is five dimensional. This reduction in dimensionality of the continuation operator results in a substantial reduction of computational and storage requirements, though at the cost of some potential loss in accuracy.

The full prestack downward continuation operator is expressed in the frequency-wavenumber domain by the Double Square Root (DSR) dispersion relation

$$\begin{aligned} k_z &= \sqrt{\frac{\omega^2}{v(\vec{\mathbf{s}},z)^2} - \frac{1}{4}\left[(k_{x_m} - k_{x_h})^2 + (k_{y_m} - k_{y_h})^2\right]} \\ &+ \sqrt{\frac{\omega^2}{v(\vec{\mathbf{g}},z)^2} - \frac{1}{4}\left[(k_{x_m} + k_{x_h})^2 + (k_{y_m} + k_{y_h})^2\right]}, \end{aligned} \tag{2}$$

where ω is the temporal frequency, k_{x_m} and k_{y_m} are the midpoint wavenumbers, and k_{x_h} and k_{y_h} are the offset wavenumbers; $v(\vec{\mathbf{s}},z)$ and $v(\vec{\mathbf{g}},z)$ are respectively the propagation velocities at the source and receiver location.

A stationary-phase approximation of the full DSR yields the common-azimuth dispersion relation. This new dispersion relation can be expressed as the cascade of two 2-D relations. The first relation is that for 2-D prestack downward-continuation

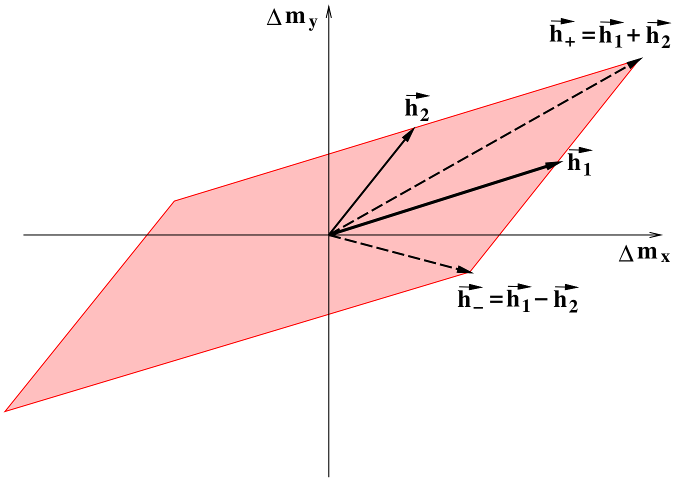

Figure 1: The maximum spatial support of the AMO operator (shaded parallelogram) in the midpoint plane $(\Delta m_x, \Delta m_y)$, as a function of the input offset $\mathbf{h}_1$, and the output offset $\mathbf{h}_2$. biondo1-amo-apert [NR]

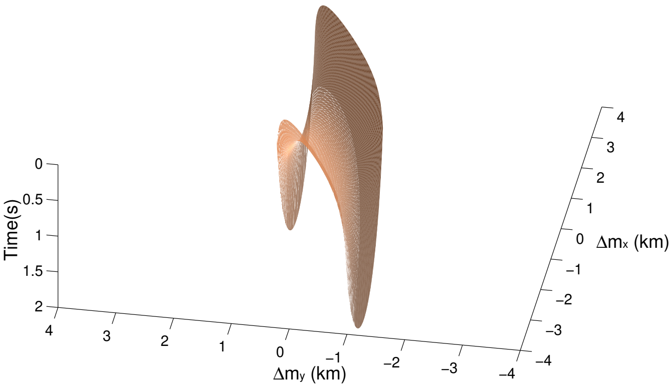

Figure 2: AMO impulse response when $t_1 = 1$ s, $h_1 = 2$ km, $h_2 = 1.8$ km, $\theta_1 = 0°$, $\theta_2 = 30°$ and no limitations are imposed on the operator aperture. biondo1-amo-max [NR]

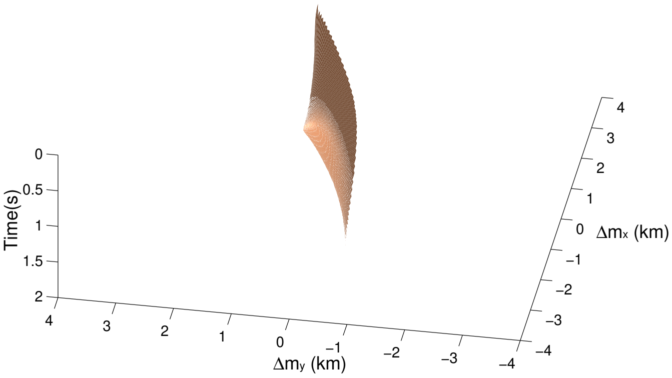

Figure 3: AMO impulse response when $t_1 = 1$ s, $h_1 = 2$ km, $h_2 = 1.8$ km, $\theta_1 = 0°$, $\theta_2 = 30°$ and the aperture is limited assuming $V_{min} = 2$ km/s. biondo1-amo-eff [NR]

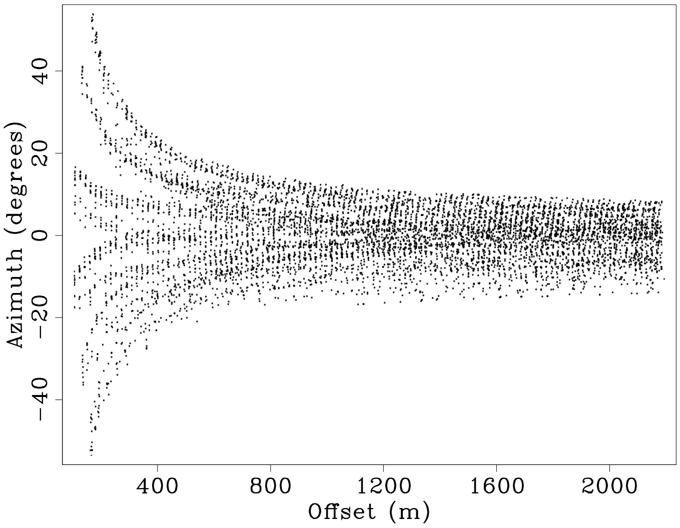

Figure 4: Offset-azimuth distribution of the test data set. The vertical bars show the boundaries among the offset ranges that were used for partial stacking. biondo1-OffAzsm [CR]

along the in-line direction,

$$k_{z_x} = \sqrt{\frac{\omega^2}{v(\vec{\mathbf{s}},z)^2} - \frac{1}{4}\left[(k_{x_m} - k_{x_h})^2\right]} + \sqrt{\frac{\omega^2}{v(\vec{\mathbf{g}},z)^2} - \frac{1}{4}\left[(k_{x_m} + k_{x_h})^2\right]} \tag{3}$$

and the second relation is the one for 2-D zero-offset downward continuation along the cross-line axis,

$$\widehat{k_z} = \sqrt{k_{z_x}^2 - k_{y_m}^2}. \tag{4}$$

The common-azimuth downward continuation operator is not as a general operator as the full DSR, and consequently it introduces some approximations. However, the components of the wavefield that contribute significantly to the final image are correctly extrapolated (Biondi and Palacharla, 1996).

COMMON-AZIMUTH IMAGING OF A MARINE DATA SET

I tested the common-azimuth imaging procedure on a data set recorded in the North Sea. The data require 3-D prestack depth migration to be properly imaged because of a shallow chalk layer with variable thickness, and a deeper salt layer with a central upswelling (Hanson and Witney, 1995). The same data set was used to test separately the two main components of the common-azimuth imaging procedure: AMO (Biondi et al., 1996) and common-azimuth migration (Biondi, 1996).

The data-acquisition configuration was dual-source and triple streamer. The nominal common-midpoint spacing was 9.375 m in the in-line direction, and 25 m in the cross-line direction. The cable length was 2,200 m, with maximum feathering of approximately 17 degrees. Figure 4 shows the offset-azimuth distribution of a small subset of the data traces. As it is typical for such acquisition geometry, the figure shows six distinct trends, which are most distinguishable at small offsets; each trend corresponding to individual source-streamer pairs.

Figure 5 demonstrates the effectiveness of the common-azimuth imaging procedure to image 3-D data in the presence of a complex velocity function. The figure shows an in-line section extracted from a migrated cube imaged by common-azimuth migration. The superposition of the migrated results onto the velocity model shows that common-azimuth migration successfully imaged the reflectors and correctly positioned them in depth. The migrated salt boundaries overlap quite precisely with the salt boundaries identified by the sharp variations in the velocity model. The target reflectors below the salt layer are also well imaged, though it seems that their focusing could be improved by further refinements of the velocity function.

Figure 6 and Figure 7 demonstrate the advantages of including AMO into the common-azimuth imaging procedure. The figures show sections extracted from image cubes obtained by common-azimuth migration. The sections on the left were obtained including AMO in the processing sequence; the ones on the right by transforming the data to common-azimuth using residual NMO followed by midpoint interpolation. To make the comparison as fair as possible to the conventional method of simple NMO-stacking, its accuracy was maximized by applying a lateral interpolation to the traces after NMO. Tests showed that this lateral interpolation preserved the dipping events significantly better than a simple binning procedure.

Figure 6 compares depth slices. The fault-plane reflections indicated by the arrows are better imaged in the results obtained by including AMO. Figure 7 compares in-line sections. The image obtained by including AMO better preserves the salt flank reflection (Arrow A) and the reflection from a dolomite rafting inside the salt layer (Arrow B). In general, the inclusion of AMO improves the accuracy of common-azimuth depth imaging, even for data sets with relatively small azimuth range. Even greater benefits should be expected for more modern data sets recorded with more than three streamers, and thus having a wider azimuthal range. To transform marine data to common azimuth a simple azimuth rotation needs to be performed by AMO; whereas, both an azimuth rotation and an offset continuation are required prior to partial stacking. Therefore, the effects of including AMO in the common-azimuth transformation are less significant than the effects of including AMO in the partial stacking process described in (Biondi et al., 1996).

COMMON-AZIMUTH VELOCITY ESTIMATION

Another attractive application of common-azimuth processing of 3-D marine data is the possibility to perform velocity estimation based on the focusing of wavefield at depth. "Focusing analysis" has been successfully applied to estimate depth-migration velocities for 2-D data (Yilmaz and Chambers, 1984; MacKay and Abma, 1992). It has some inherent advantages with respect to velocity estimation based on coherency of migrated events across offsets, that is the criterion routinely used in conjunction with Kirchhoff prestack migration. Residual moveout applied to migrated constant-offset data is only a partial residual focusing operator, since it does not refocus the data along the midpoint axes. By contrast, focusing analysis based on downward-

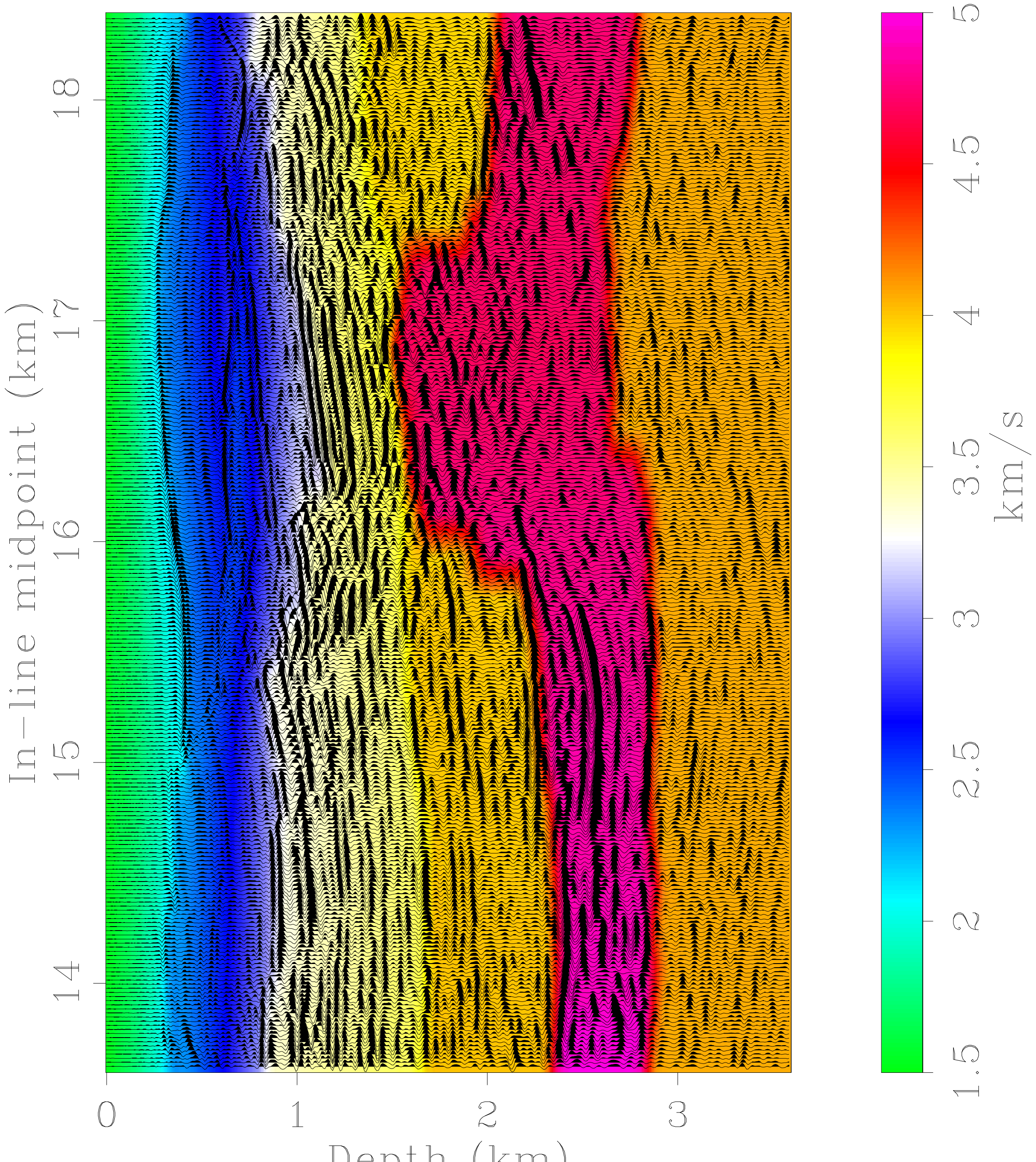

Figure 5: In-line section extracted from a migrated cube imaged by common-azimuth migration. The wiggle plot is superimposed onto a plot of the velocity model. biondo1-veldata19800 [CR]

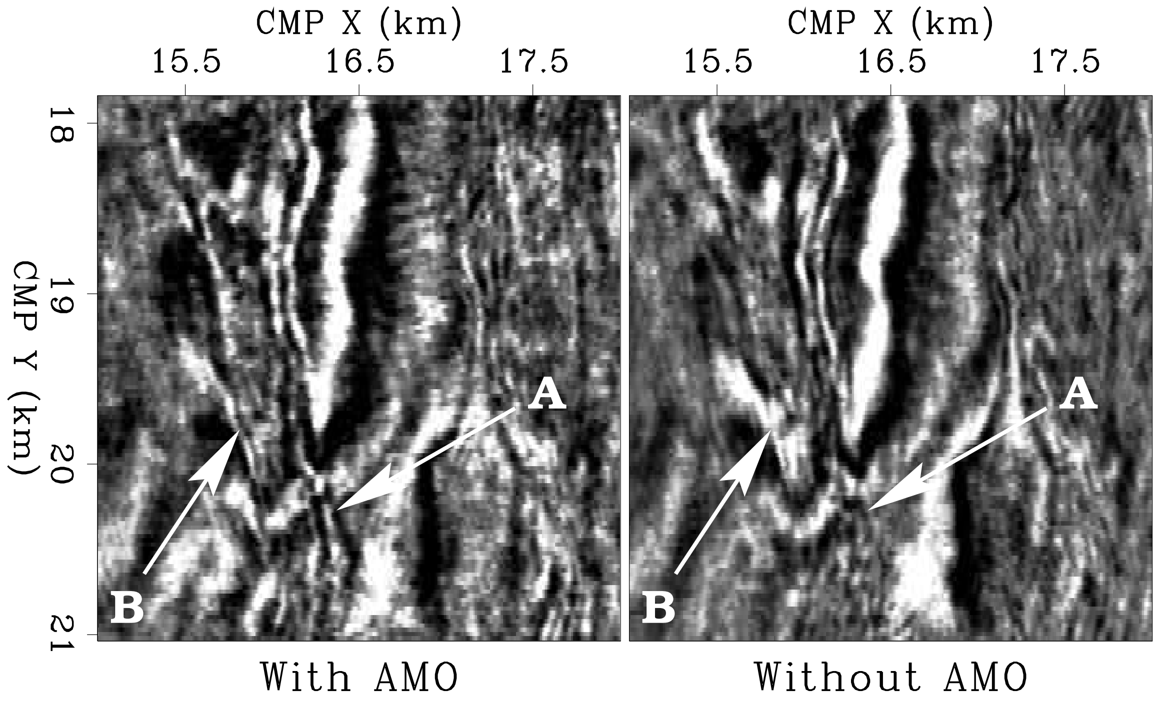

Figure 6: Depth-slices extracted from two cubes imaged by common-azimuth migration. Including AMO (left) and not including AMO (right). biondo1-dslice-1288-arr [CR]

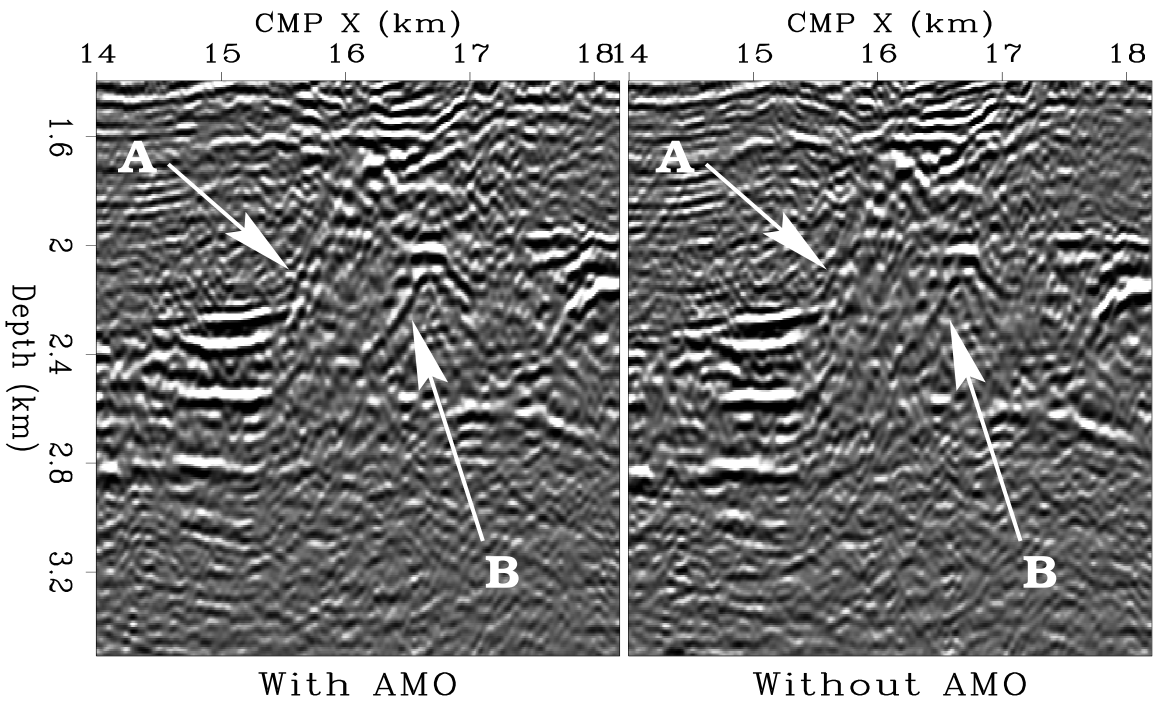

Figure 7: In-line sections extracted from two cubes imaged by common-azimuth migration. Including AMO (left) and not including AMO (right). biondo1-xslice-18950-arr [CR]

continuation operators does include a midpoint component. Because of these inherent advantages, velocity-estimation methods based on wavefield focusing, have been revived lately and proposed for 3-D velocity estimation as Common Focal Point (CFP) methods (Kabir and Verschuur, 1996; Morton and Thorbecke, 1996). However, the straightforward application of CFP methods to 3-D data with arbitrary geometry could be extremely computationally intensive. Whereas, the application of CFP methods to marine data using the common-azimuth imaging tools described in this paper would be computationally efficient, and thus they could become practical methods to estimate velocity for 3-D prestack depth imaging of a wide class of marine data sets.

CONCLUSIONS

The proposed common-azimuth procedure was successful in prestack depth imaging a 3-D marine data set recorded over a complex geological area. The results presented in this paper demonstrate that the application of AMO in conjunction with common-azimuth migration is a viable method for full-volume prestack imaging.

The transformation of the recorded data to effective common-azimuth data by AMO improves the final image even when the data was acquired with only three streamers. Consequently, AMO should to be included for the accurate common-azimuth imaging of modern data sets acquired with more than three streamers.

The introduction of common-azimuth imaging opens several promising new possibilities for velocity estimation based on wavefield focusing.

ACKNOWLEDGEMENTS

I would like to thank Conoco and its partners BP and Mobil, for agreeing to release the data. The research presented in this paper was funded by the sponsors of the Stanford Exploration Project and by the ACTI project # 4731U0015-3Q.

REFERENCES

Albertin, U., Cabrera, J., Chang, W., Fowler, P., Stankovic, G., and Ward, L., 1996, A comparison of Kirchhoff migration results for the SEG/EAGE salt model using several traveltime generators: 66th Ann. Internat. Meeting, Soc. Expl. Geophys., Expanded Abstracts, 562–565.

Biondi, B., and Palacharla, G., 1996, 3-D prestack migration of common-azimuth data: Geophysics, **61**, 1822–1832.

Biondi, B., Fomel, S., and Chemingui, N., 1996a, Azimuth moveout for 3-D prestack imaging: Submitted to Geophysics.

Biondi, B., Fomel, S., and Chemingui, N., 1996b, Azimuth moveout for 3-D prestack imaging: SEP–**93**, 15–44.

Biondi, B., 1996, Common-azimuth prestack depth migration of a North Sea data set: SEP–**93**, 1–14.

Geoltrain, S., and Brac, J., 1993, Can we image complex structures with first-arrival traveltime?: Geophysics, **58**, no. 4, 564–575.

Godfrey, B., Pieprzak, A., Berg, K., and Yilmaz, O., 1993, 3-D Salt and sub-salt imaging strategy: A case history from the Gulf of Mexico: 3-D Seismology: Integrated Comprehension of Large Data Volumes – SEG Summer Research Workshop.

Hanson, D. W., and Witney, S. A., 1995, 3-D prestack depth migration – velocity model building and case history: 1995 Spring Symposium of the Geophys. Soc. of Tulsa, Soc. Expl. Geophys., Seismic Depth Estimation, 27–52.

Kabir, M. M. N., and Verschuur, D. J., 1996, Migration velocity analysis using the common focus point technology: 66th Ann. Internat. Meeting, Soc. Expl. Geophys., Expanded Abstracts, 407–410.

MacKay, S., and Abma, R., 1992, Imaging and velocity estimation with depth-focusing analysis: Geophysics, **57**, no. 12, 1608–1622.

Morton, S., and Thorbecke, J., 1996, Automating prestack migration analysis using common focal point gathers: 66th Ann. Internat. Meeting, Soc. Expl. Geophys., Expanded Abstracts, 411–414.

Nichols, D. E., 1996, Maximum energy traveltimes calculated in the seismic frequency band: Geophysics, **61**, 253–263.

Yilmaz, O., and Chambers, R., 1984, Migration velocity analysis by wave-field extrapolation: Geophysics, **49**, no. 10, 1664–1674.